Nano Energy 140 (2025) 111007

Contents lists available at ScienceDirect

Nano Energy

journal homepage: www.elsevier.com/locate/nanoen

Full paper

Octopus-inspired soft gripper with embedded triboelectric tactile sensor for underwater target recognition and grasp

Hongyi Chen [a,1], Yuanzheng Li [a,1], Peng Xu [b,*], Jiaqian Li [a], Aziz Noor [a], Xinyue Zhou [a], Weichao He [a], Tianrun Wang [a], Zhaoyang Mou [a], Liguo Song [a,*], Minyi Xu [a,*]

[a] State Key Lab of Maritime Technology and Safety, Marine Engineering College, Dalian Maritime University, Dalian 116026, China
[b] Intelligent Biomimetic Design Lab, College of Engineering, Peking University, Beijing 100871, China

ARTICLE INFO

Keywords:
Underwater soft gripper
Bionic Octopus
Triboelectric nanogenerator
Tactile sensor

ABSTRACT

In underwater salvage operations, robotic grippers with high sensitivity and stable clamping performance significantly enhance retrieval efficiency while ensuring the integrity of target objects. Octopuses can accurately perceive information of grasped objects through their arms and dorsal membranes, utilizing suction cups for precise object capture. Inspired by these sensing and grasping mechanisms, this paper proposes a bionic underwater octopus tactile gripper (UOTG) based on the triboelectric nanogenerator. The UOTG mainly features a network of suction cup-like structures and embedded triboelectric sensors, which enable it to sense external stimuli in underwater low-visibility and noisy environments. Its fully soft structure facilitates adaptation to varying object shapes and sizes. The triboelectric sensor array generates electrical signals through contact-separation effects, providing tactile information regarding the pressure and deformation of objects being grasped. Notably, the incorporation of MXene, a novel functional material, into the sensing unit of UOTG significantly enhances charge transfer efficiency and sensor sensitivity while ensuring stable tactile perception performance in complex underwater environments. The UOTG demonstrates a linear sensitivity to grasping force and is capable of detecting object detachment, estimating object volume, and identifying object shape and hardness. Experimental results reveal recognition accuracies of 98.3 % and 98.0 % for object shape and hardness, respectively. These findings demonstrate that the UOTG enhances underwater sensing capabilities and holds great potential for applications in underwater grasping and salvage operations.

1. Introduction

Remotely operated vehicles (ROVs) serve as essential tools in advancing modern marine activities and research [1–7]. Compared to traditional manual exploration methods, ROVs offer enhanced flexibility and precision while significantly reducing the risk of underwater hazards for divers [8]. ROVs equipped with grippers enable efficient grasping and salvage operations, making them widely applicable in various underwater fields, including underwater archaeology [9], sample acquisition [10], and underwater accident investigation [11]. Accurately obtaining information about the target object and precisely controlling the grasping force are critical factors for achieving non-destructive grasping [12]. Although optical sensors [13] and sonar sensors [14] can assist grippers in performing underwater grasping tasks, their effectiveness is hindered by challenges such as low-light conditions and strong interference noise in the marine environment, which limits grasping efficiency. In this context, underwater tactile sensing serves as a critical supplementary perception technology, offering more reliable feedback and enhancing the perceptual dimensions of underwater grasping [15,16]. This enables grippers to perform more precise grasping operations in complex underwater environments [17]. Consequently, the integration of underwater tactile sensing with existing sensor technologies and the development of a tactile feedback sensor specifically designed for underwater grasping have emerged as critical challenges that required attention [18].

In the marine environment with low-light conditions and strong interference noise, marine organisms can use tactile sensation to obtain surrounding information [19]. For instance, the glowing sucker octopus and vampire squid perform precise and non-destructive grasping with their arms while also sensing the shape, hardness, texture and other

* Corresponding authors.
E-mail addresses: pengxu@pku.edu.cn (P. Xu), songliguo@dlmu.edu.cn (L. Song), xuminyi@dlmu.edu.cn (M. Xu).
[1] These authors contributed equally to this work

https://doi.org/10.1016/j.nanoen.2025.111007
Received 6 January 2025; Received in revised form 28 March 2025; Accepted 12 April 2025
Available online 14 April 2025
2211-2855/© 2025 Elsevier Ltd. All rights are reserved, including those for text and data mining, AI training, and similar technologies.

properties of the grasped objects [20]. This ability greatly aids in tasks such as foraging and avoiding predators in complex marine environments [21]. Further research has revealed that the behavior of the glowing sucker octopus is facilitated by the unique soft tissue dorsal membrane structure on its tentacles [22]. As illustrated in Fig. 1a, this structure enhances the flexibility and adaptability of the suction cup while enabling the tentacle to accurately detect subtle tactile signals during contact with an object. The softness and elasticity of the dorsal membrane allow the suction cup to efficiently grasp objects with varying shapes and hardness. Additionally, it provides sensitive feedback on surface details, enabling the optimization of grasping force and technique. Inspired by this, Wu's team developed a bionic soft gripper in 2022 [23], compared to traditional finger-shaped grippers, this innovative design enhances grasping stability through the incorporation of suction cups and bionic octopus dorsal membranes, while also demonstrating the ability to adapt to objects of varying shapes and properties. These findings demonstrate that bionic design can effectively replicate the intricate structures and functions of natural organisms, offering more efficient and flexible solutions for the development of underwater tactile sensors [24].

To endow the soft gripper with underwater tactile perception, the tactile sensing framework based on triboelectric nanogenerator (TENG) was optimized for the underwater environment. Novel functional materials were incorporated into the sensing units to enhance the tactile sensing performance. TENG combines triboelectric and electrostatic induction effects[25–27]. When two different materials come into contact, the transfer of electrons will cause charge separation on the surface of the materials, thereby forming a voltage difference [28]. This voltage difference can drive electrons to flow in the external circuit, thereby generating current. With its high sensitivity and simple structure, TENG technology has found extensive applications in underwater self-powered tactile sensing [29]. For instance, in 2022, Wang's team developed a fish motion behavior monitoring device based on TENG technology [30], while in 2024, Li's team introduced an underwater target shape recognition device utilizing the same technology [31]. Furthermore, self-powered triboelectric sensors are capable of detecting pressure changes in catheter balloons within the body [32] and responding to external variations in pressure, acceleration, force, and rotational motion [33]. The contact-separation TENG utilizing ink layers and FEP layers as electrodes, can be fabricated into a highly sensitive flexible sensor [34]. Furthermore, as an emerging functional material, MXene (Ti_3C_2Tx) possesses abundant surface functional groups (-OH, -O, etc.), which not only facilitate charge transfer but also enhance interfacial bonding with the elastomer via hydrogen bonding—an essential factor

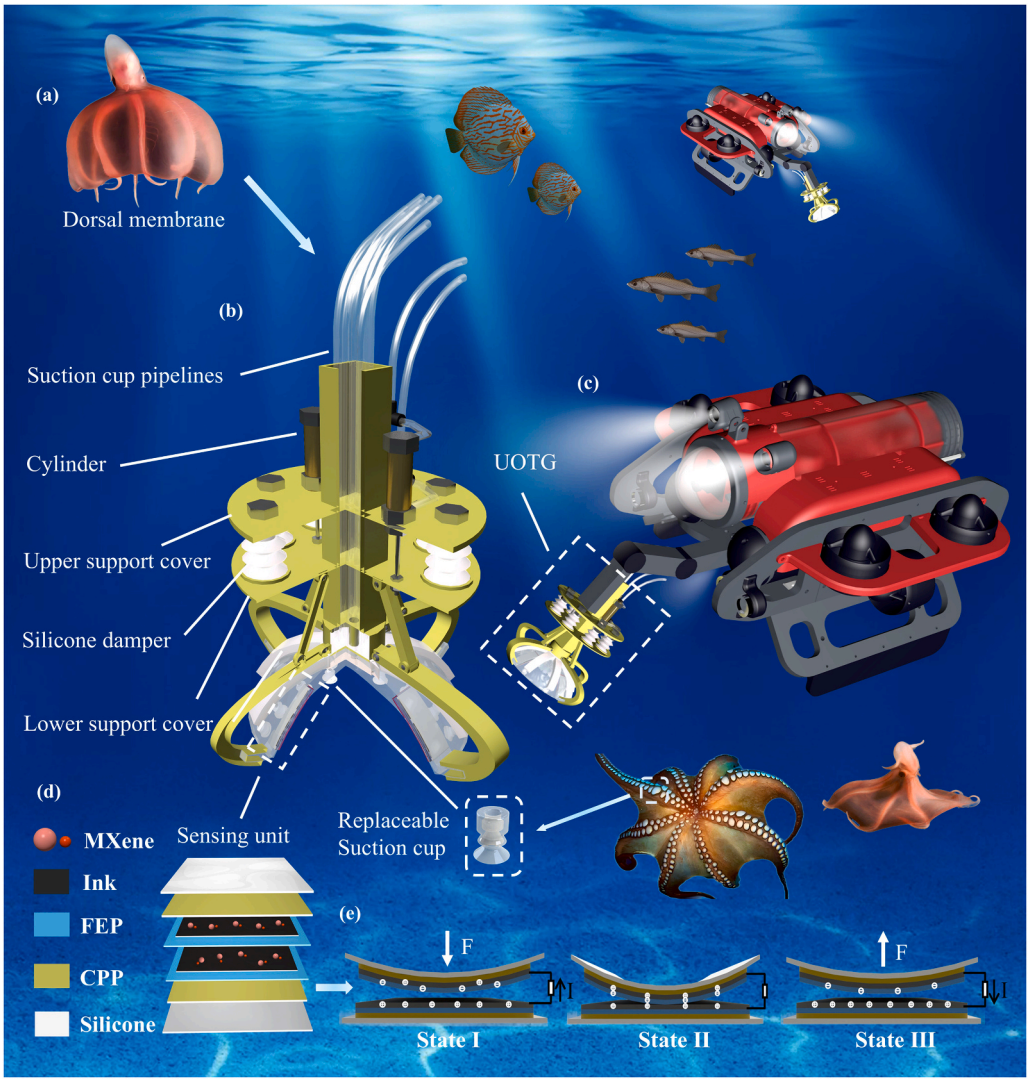

Fig. 1. Design concept and working mechanism of UOTG. a Dorsal membrane. b Structure of UOTG. c Schematic diagram of the effect of UOTG installed on ROV. d Schematic diagram of the material layer structure of the sensing unit. e Contact-separation and charge transfer process of sensing unit under external force stimulation.

in ensuring the long-term stability of the sensor in underwater environments. Consequently, incorporating MXene into the ink layer of the original sensing unit significantly enhances its sensing performance. This new sensing unit is now integrated into the soft gripper, enabling a more biomimetic replication of the octopus's tactile perception.

Here, we integrated the contact-separation TENG with the dorsal membrane and tentacle structures of octopus to develop a bionic underwater octopus tactile gripper (UOTG). In addition to its ability to stably grasp target objects, the gripper is capable of providing feedback on grasping force, detecting object detachment, estimating object size, and identifying the shape and hardness of the grasped object. As illustrated in Fig. 1b, the UOTG primarily consists of suction cup pipelines, cylinders, support covers, silicone dampers, and a silicone dorsal membrane embedded with four sensing units. Based on the soft gripper developed by Xie's team [23], the UOTG introduces structural innovations through several key enhancements: reduced air leakage in suction cups, replaceable suction cup configuration, innovative self-suction capability, and an optimized gripping mechanism. During the gripping process, the UOTG wraps objects with the assistance of suction force generated by a pump and deformation of the silicone dorsal membrane. During this phase, the sensing unit undergoes compression, inducing a contact-separation effect that generates an electrical signal. The UOTG demonstrates a linear sensitivity to grasping force ($S = 0.0566\ F - 0.1510\ V/N$) and its recognition accuracy for object shape and hardness reaches 98.3 % and 98.0 % respectively. The results demonstrate that the UOTG exhibits high-precision perception and grasping capabilities in complex underwater environments, significantly enhancing the reliability and intelligence of underwater grasping tasks. This innovative technology holds great potential for future applications in intelligent marine grasping operations.

2. Results and discussion

2.1. Basic structure and working mechanism of UOTG sensing unit

The UOTG can be integrated on ROVs to acquire detailed information about the grasped object through direct contact. The specific application is illustrated in Fig. 1c. The sensing functionality of UOTG is primarily enabled by its specialized sensing unit, the structure of which is depicted in Fig. 1d. This tactile sensing unit is composed of silicone, cast polypropylene (CPP) films, MXene-enhanced conductive ink, and fluorinated ethylene propylene (FEP) films. The MXene-enhanced ink layer serves as the positive electrode, while the FEP layer acts as the negative electrode. Both layers are encapsulated within a 1 mm thick CPP shielding layer to mitigate underwater interference signals. Additionally, an outer silicone encapsulation further enhances the waterproofing and interference resistance of the sensing unit. Notably, the placement order of the ink and FEP layers is critical, as reversing them would disrupt the electrode polarity, preventing the generation of electrical signals. Ink and FEP materials were selected to form the positive and negative electrodes of the sensing unit due to their significant difference in electronegativity, which generates a large potential difference, thereby enhancing signal output (Figure S7 in the supplementary material illustrates the electronegativity gap of common materials). Furthermore, while ensuring long-term stable operation, the choice of ink and FEP effectively reduces material costs and simplifies the manufacturing process, making the sensing unit more economically viable. Building on this, the incorporation of MXene (Ti_3C_2Tx) substantially improves the conductivity and charge transfer efficiency of the sensing unit, further enhancing both signal strength and sensing sensitivity. This optimized design not only improves the overall performance of the sensing unit but also balances cost control and manufacturability, ensuring efficient signal output and providing a more reliable solution for underwater tactile sensing applications.

Fig. 1e shows the electron transfer process of the sensing unit receiving external stimulation. The FEP film is in contact with the ink electrode, causing the electron cloud to overlap on the two layers. Since FEP has a greater electronegativity than ink, the electrons of the ink layer enter the deeper potential well of the FEP film. That is, the lowest molecular orbital at the FEP interface acquires free electrons from the ink surface. When the sensing unit removes the external load, the FEP film separates from the ink electrode. Since the positive and negative friction charges no longer coincide on the same plane, a dipole moment and potential are generated between the two contact surfaces. Therefore, to balance the local electric field, the free electrons are transferred through the external circuit, thereby generating positive charges on the conductive ink electrode. The flow of electrons continues until the distance between the two contact surfaces reaches a maximum value. Simultaneously, the voltage difference decreases, and the free electrons return through the external circuit. Finally, the charge distribution returns to the initial state, completing the entire power generation cycle. External force can be converted into deformation by the triboelectric sensing unit. Charge transfer occurs during the deformation process.

2.2. Composition and fabrication method of the UOTG

Building upon the soft gripper designed by Xie's team [23], the UOTG has been upgraded with multiple improvements, including reduced air leakage in the suction cups, a replaceable suction cup design, an optimized gripping mechanism, innovative self-suction capability, and significantly enhanced tactile sensing performance. Fig. 2a presents a schematic of the physical experiment with the UOTG, which consists primarily of an upper mechanical driver and a lower backing film. Compared to the previous soft gripper, the UOTG optimizes the internal air pipe structure, reducing the negative effects of air leakage on both the grasping and sensing processes. Additionally, a replaceable suction cup design has been incorporated, allowing for suction cups of varying sizes and shapes to be swapped depending on the target object. Furthermore, the driving mechanism of the UOTG differs significantly from that of the previous soft gripper, utilizing a small cylinder for actuation, which enhances grasping speed compared to the bellows-driven system. Multiple silicone dampers are employed to minimize the impact force of the cylinder, and by connecting the suction pipe to the upper connector of the silicone damper, automatic suction during the grasping process is achieved without the need for an external suction source. The structure of the mechanical driver is shown in Fig. 2b, it primarily consists of suction cup pipelines, cylinders, support covers, silicone dampers, connecting rod and so on. The function of mechanical driver is to adjust the angle of the connecting rod using an external air pump, thereby controlling the opening and closing of the dorsal membrane. Fig. 2c is the injection 3D mold of the silicone dorsal membrane, it consists of eight combined and detachable parts. The four bottom molds are used to make the bionic silicone dorsal membrane, and the hollow joints for the replaceable suction cups, while the four top molds are used to make the bionic arms and create the internal suction cup airways. Fig. 2d shows the production process of UOTG. The assembly process begins by integrating eight connecting rods with the hollow column to form the mechanism driver. Subsequently, the lower cover plate equipped with a damping suction cup is threaded through the hollow column and secured to the connecting rod. Ultimately, the upper cover plate is affixed to the damping suction cup apex, followed by the installation of the cylinder, cylinder tube, and angle sensor onto the hollow column assembly.

The octopus back membrane exhibits exceptional softness, with a Shore hardness of approximately 10 A [35]. To replicate its mechanical properties as accurately as possible, it is essential to select a soft material with a comparable Shore hardness. Dragon Skin 10, a soft silicone elastomer, offers an adjustable hardness ranging from 5 A to 15 A depending on the mixing ratio, making it an ideal candidate for fabricating biomimetic back membranes. Mix the appropriate amount of liquid A and liquid B in a beaker, then place the mixture in a vacuum environment for a period of time to remove any bubbles formed during

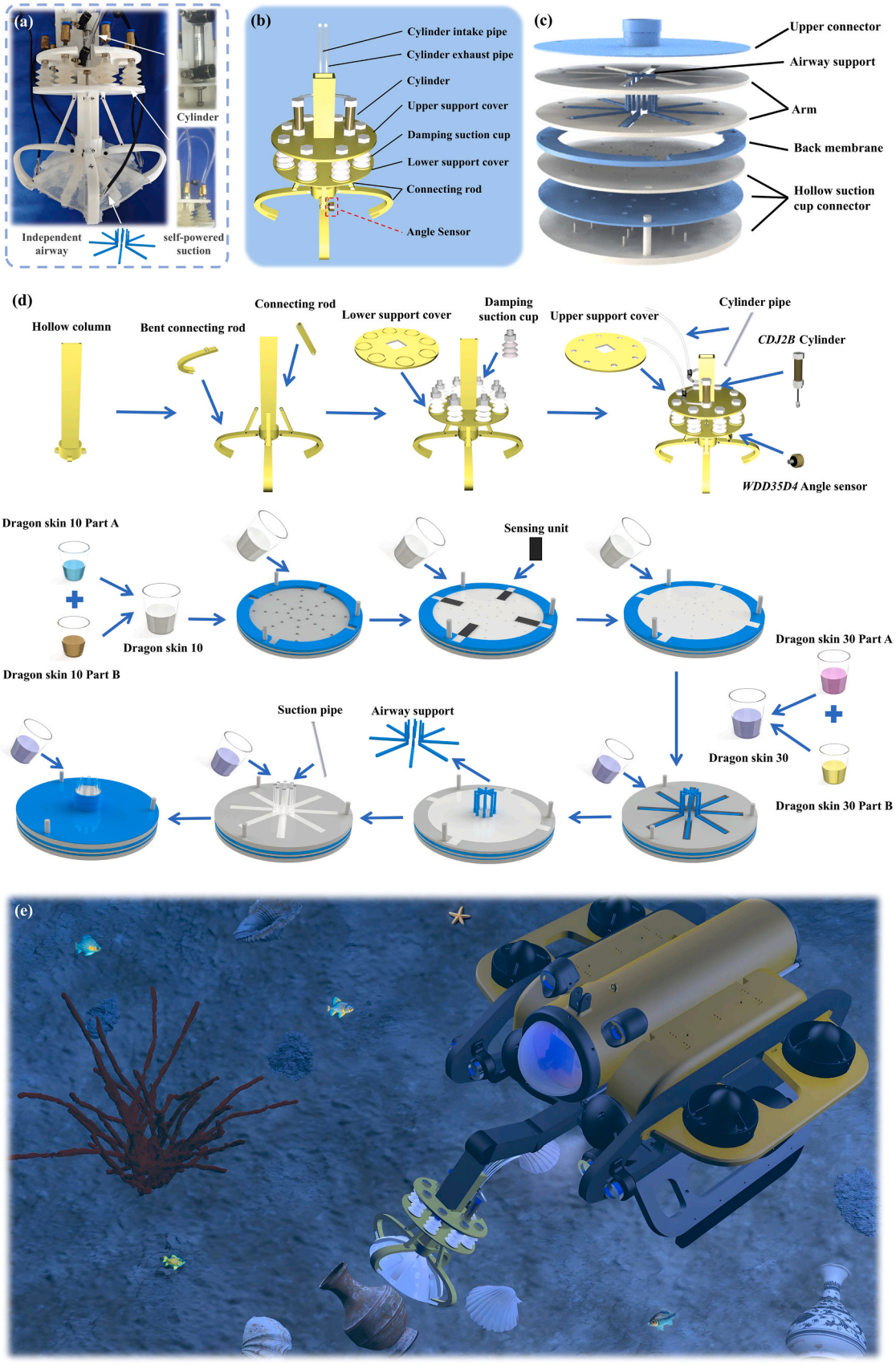

Fig. 2. Composition and fabrication method of the UOTG. a The real experimental image of the UOTG. b Basic structure of UOTG drive device. c Silicone mold composition of soft gripper. d Detailed manufacturing process of UOTG. e Application of UOTG in underwater installed on ROVs.

the mixing and stirring process. When the mixture is pumped in vacuum, pour the mixture into the mold manufactured by 3D printing. When the soft gripper is made, the bottom four molds are combined, stop adding silicone when it reaches a depth of 3 mm on the top surface of the mold. After the silicone dries, place four sensor units at 90° intervals, and then continue to add silicone until it reaches the top of the mold surface. Imitation of the octopus's arms and body with high hardness, the airways and connecting parts are made of Dragon skin 30 with high hardness. Dragon Skin 30 is mixed with A and B, and the process is consistent with Dragon Skin 10. In addition, the airway supporting parts of Vaseline and the combination of bionic octopus arm mold combinations are used to pour Dragon Skin 30. It should be noted that the top of

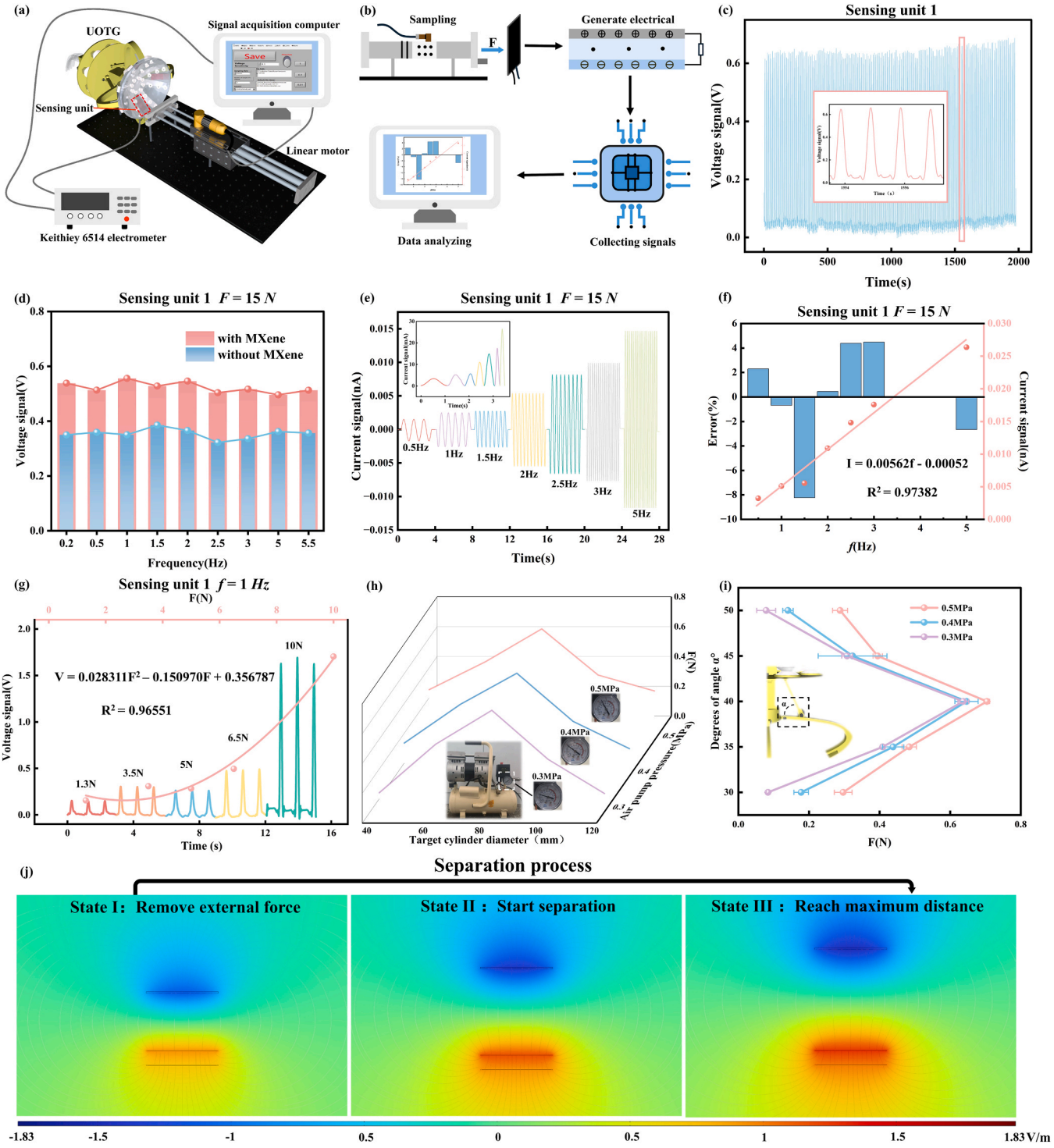

Fig. 3. Sensing unit test experiment and the output characteristics of UOTG. a The experimental bench of UOTG. b Schematic diagram of the electromechanical conversion principle of UOTG. c The stability test of UOTG during 2000 s d The open-circuit voltage of the sensing unit with and without MXene material was measured under stimulation at different frequencies while maintaining a fixed pressure of F = 15 N. e The short circuit current of the sensing unit when stimulated at different frequencies at a fixed pressure of F = 15 N. f Current relationship corresponding to different frequency loads of the sensing unit. g Relationship between output voltage and load pressure of UOTG. h Relationship between target cylinder diameter and grip force. i Relationship between different connecting rod angles α. j Simulation analysis of charge transfer during sensing unit separation.

the small pillar of the bottom mold needs to be closely fitted with the bottom of the airway support mold to create a continuous and smooth channel. When the silicone dries, cut off the top connectors of the airway support mold separately. Using the characteristics of strong silicone deformation capabilities, remove the separation support. Then eight suction cup pipelines were laid out in the hollow where the supports were removed, and finally the uppermost mold was filled with silicone to secure the pipelines while creating a connection to the mechanical drive. Finally, remove the mold, take out the soft gripper, and install the small suction cup to connect to the suction cup connection port to complete the production of the soft gripper. Soft gripper has a certain degree of flexibility to achieve scalability and adaptive grabbing ability. After the soft gripper is made, pass the pipelines through the hollow column. Fix the top connector of the soft gripper and the four symmetrical square connectors on the outside to the drive device. Inject an appropriate amount of Dragon Skin 30 into the central hollow pillar from the top to make the connection between the soft gripper and the drive device more stable. Once the silicone has cured, the UOTG is complete. Fig. 2e is a simulation diagram of an ROV equipped with UOTG for underwater grabbing applications.

2.3. The output characteristics of UOTG

Fig. 3a shows the onshore test bench of UOTG, which includes a linear motor, an *LZ-WL2* pressure sensor with an intelligent display instrument, a *Keithley 6514* electrometer, and a computer for collecting data. During the experiment, the UOTG was placed flat and fixed to ensure its sensing unit was aligned with the linear motor. The linear motion of the motor was then used to simulate the variations in external pressure. Fig. 3b shows the electromechanical conversion principle of UOTG, the linear motor strikes the sensing unit at a fixed frequency, causing deformation due to applied force, which results in contact separation and the generation of electrical signals. The *Keithley 6514* electrometer is then used to collect these signals, with the data being displayed in real-time on a computer. To ensure the stability and repeatability of experimental results, a 30-minute collision test was conducted on the UOTG sensing unit prior to the formal experiments. The experiment maintained the operating frequency of the linear motor at $f = 1$ *Hz* and the impact pressure at $F = 5$ *N* , with the results shown in Fig. 3c. The data demonstrate that the output signal of the UOTG exhibits consistent characteristics and amplitude, confirming the stability of the sensing unit during continuous operation. Because of the low-frequency operating conditions, the sensing unit fully returns to its initial state after each contact-separation cycle, eliminating cumulative effects. This ensures the reliability and accuracy of the subsequent experimental data.

Fig. 3d presents the open-circuit voltage of the UOTG under different frequencies ranging from 0.2 *Hz* to 5.5 Hz while maintaining a fixed pressure of $F = 15$ *N*. The data reveal that the output voltage remains largely unchanged as the frequency varies. This is attributed to the fixed degree of contact-separation within the sensing unit under a constant external load. Since frequency variations do not alter the separation distance between the electrodes, the open-circuit voltage remains stable. In addition, a comparative analysis of the voltage output was conducted between the sensing units with and without the incorporation of MXene. The results clearly demonstrate that the addition of MXene significantly enhances the output performance of the sensing unit. In contrast, Fig. 3e illustrates the relationship between frequency and the short circuit current of the UOTG under a constant external load. The results demonstrate that as the frequency increases, the short-circuit current rises correspondingly. This is because higher frequencies accelerate the contact-separation process, leading to faster changes in the electric field and, consequently, an increase in displacement current. Therefore, under a fixed external load, the short circuit current of the UOTG increases with frequency. Additionally, Fig. 3e also highlights the sensing unit's response time across different frequencies. The data confirm that the UOTG maintains its responsiveness even at higher frequencies, establishing its potential for adapting to high-frequency underwater operations. Fig. 3f presents the mathematical relationship between the current I and the collision frequency f. The results indicate a linear correlation described by the equation $I = 0.00562\,f - 0.00052$, with a high regression coefficient of $R^2 = 0.98682$, demonstrating the strong predictive accuracy of the model.

Fig. 3g illustrates the increase in the output voltage of the sensing unit as the vertical external stimulus, applied at the frequency of 1 *Hz*, increases from 1 *N* to 10 *N*. The relationship between the voltage V and the pressure F is characterized by the quadratic equation $V = 0.028311\,F^2 - 0.150970\,F + 0.3356787$, with a regression coefficient of $R^2 = 0.98275$, indicating a high degree of fit and reliability in the model. It can be concluded that the voltage output of the sensing unit exhibits a significant upward trend as the external pressure increases. This phenomenon occurs because the higher external load reduces the distance between the electrodes, leading to the more complete contact-separation cycle and thereby enhancing the output voltage. By calculation, it is determined that when $F \leq 10$ *N*, the sensitivity of the sensing unit is expressed as $S = 0.0566F - 0.1510$ *V/N*. The experimental results demonstrate that the UOTG provides reliable mechanical feedback during grasping, exhibiting high sensitivity and stability. These characteristics enable the precise determination of parameters such as grasping frequency, highlighting the gripper's effectiveness in practical applications.

To optimize the control of the UOTG's gripping force, strength calibration was conducted. The operational range of the UOTG is constrained to objects with diameters between 40 mm and 120 mm due to the stroke limitations of the power cylinder. Hence, cylinders with diameters ranging from 40 to 120 mm were selected, and pressure sensors were mounted on them. The gripping force of the UOTG was measured on cylinders of varying diameters under air compressor driving pressures between 0.3 MPa and 0.5 MPa. The results of these measurements are presented in Fig. 3h. The results show that when grabbing cylinders of the same diameter, the greater air compressor pressure, the greater the gripping force generated. Grasping an 80 mm cylinder under the same air pressure provided by the air compressor will produce the greatest gripping force. In addition, when grasping cylinders of different diameters, the connecting rod angle α can be obtained through the angle sensor installed on the connecting rod. From this, the gripping force generated by different opening angles of the UOTG can be obtained when the air pressure driving the air compressor is 0.3–0.5 MPa, the specific results are shown in Fig. 3i. Fig. 3j presents a simulation analysis of charge transfer during the separation process of the sensing unit, conducted using COMSOL software, which illustrates the potential distribution and validates the working principle of the system. When the external force acting on the sensor unit is removed, the distance between its upper and lower electrodes gradually increases. The blue region represents the transfer of negative charges, while the red region indicates the transfer of positive charges. Initially, the charge transfer is minimal; however, as the electrode separation increases, the overall charge transfer progressively rises, illustrating the dynamic behavior of the triboelectric effect during the separation process. This simulation result aligns well with the theoretical principles of triboelectric nanogenerators, where charge transfer is influenced by the separation distance between contact surfaces and the strength of the electric field. These findings further validate the sensitivity and reliability of the sensor unit in detecting and quantifying mechanical stimuli, demonstrating its effectiveness for practical applications.

2.4. Recognition of underwater target hardness and shape

Fig. 4a shows the underwater experimental platform of UOTG, which includes an optical plate, a fixed bracket, a vacuum pump, an air compressor, a signal collection box, and a computer for data processing. This experiment utilized three silicone balls with varying hardness:

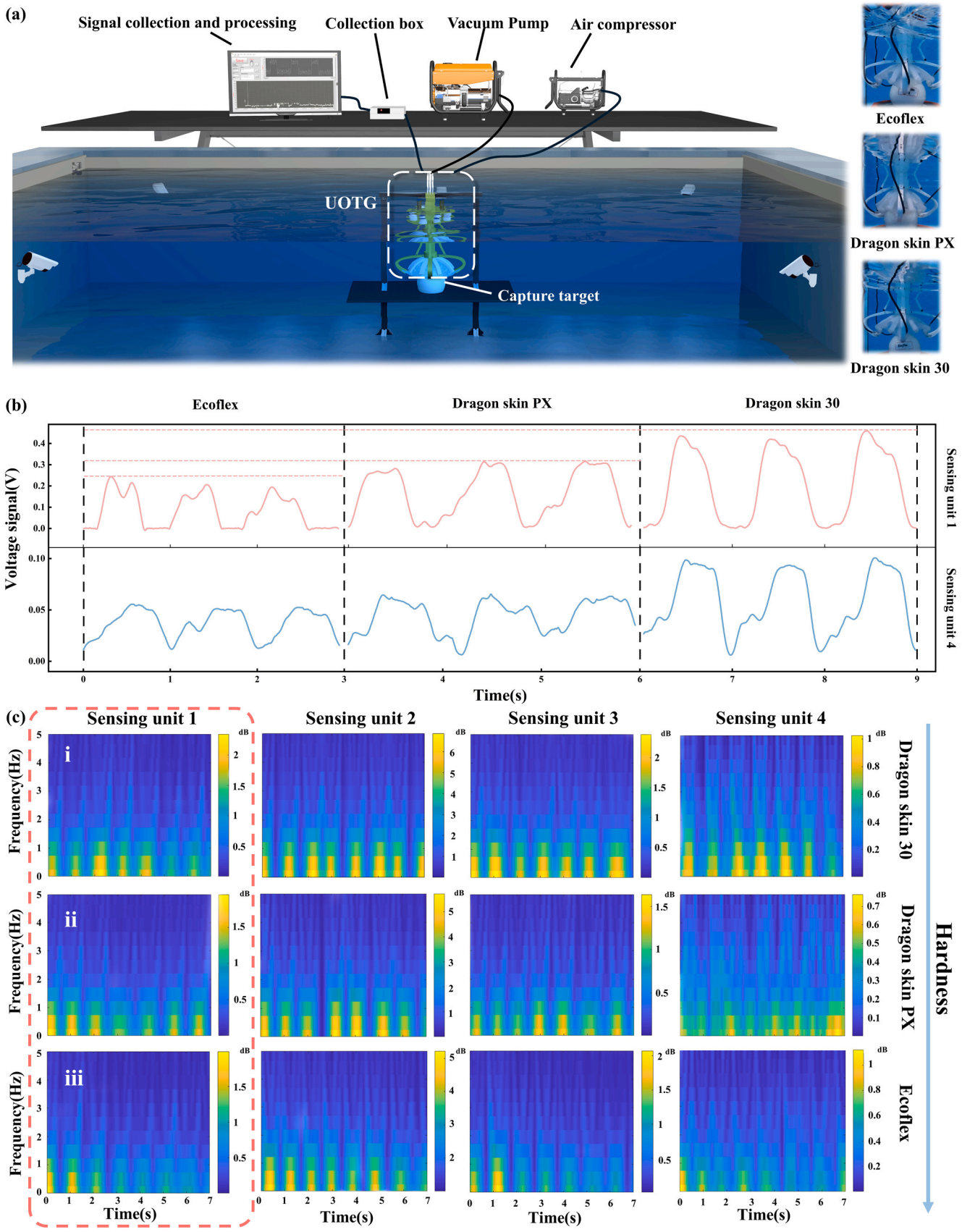

Fig. 4. Underwater hardness identification experiment of UOTG. a Underwater experimental platform of UOTG. b The Output voltage of UOTG when grasping objects of different hardness. c Time-frequency diagram of the sensing unit when UOTG grasps objects of different hardness.

Dragon Skin 30, Dragon Skin PX, and Ecoflex, with hardness decreasing progressively. The hardness of Dragon Skin 30 is approximately Shore 30 A, while Dragon Skin PX ranges from Shore 10 A to 15 A, and Ecoflex has a Shore hardness of around 5 A (specific parameters is in Supplementary Materials Figure S6) For three silicone balls of the same diameter, under the same driving pressure from the air compressor, the gripping force generated by the UOTG remains constant. Therefore, a harder target object will cause a greater deformation of the sensing unit. This enables more complete contact and separation of the sensing unit, resulting in a larger electrical signal output. Based on this, we can predict the experimental results before conducting the hardness identification experiment: Dragon Skin 30 should have the highest voltage output signal, followed by Dragon Skin PX, with Ecoflex generating the lowest voltage output signal. Fig. 4b presents the voltage output from the grasping experiment conducted under the same air compressor driving pressure of 0.5 MPa. The experimental results align with the previous predictions, confirming the expected trend.

Fig. 4c illustrates the time-frequency diagram of the voltage signal generated by the sensing unit when the UOTG grasps objects of varying hardness. The color gradient, from blue to yellow, represents signal strength, with blue indicating low signal strength and yellow indicating high signal strength. When grasping materials of different hardness, the

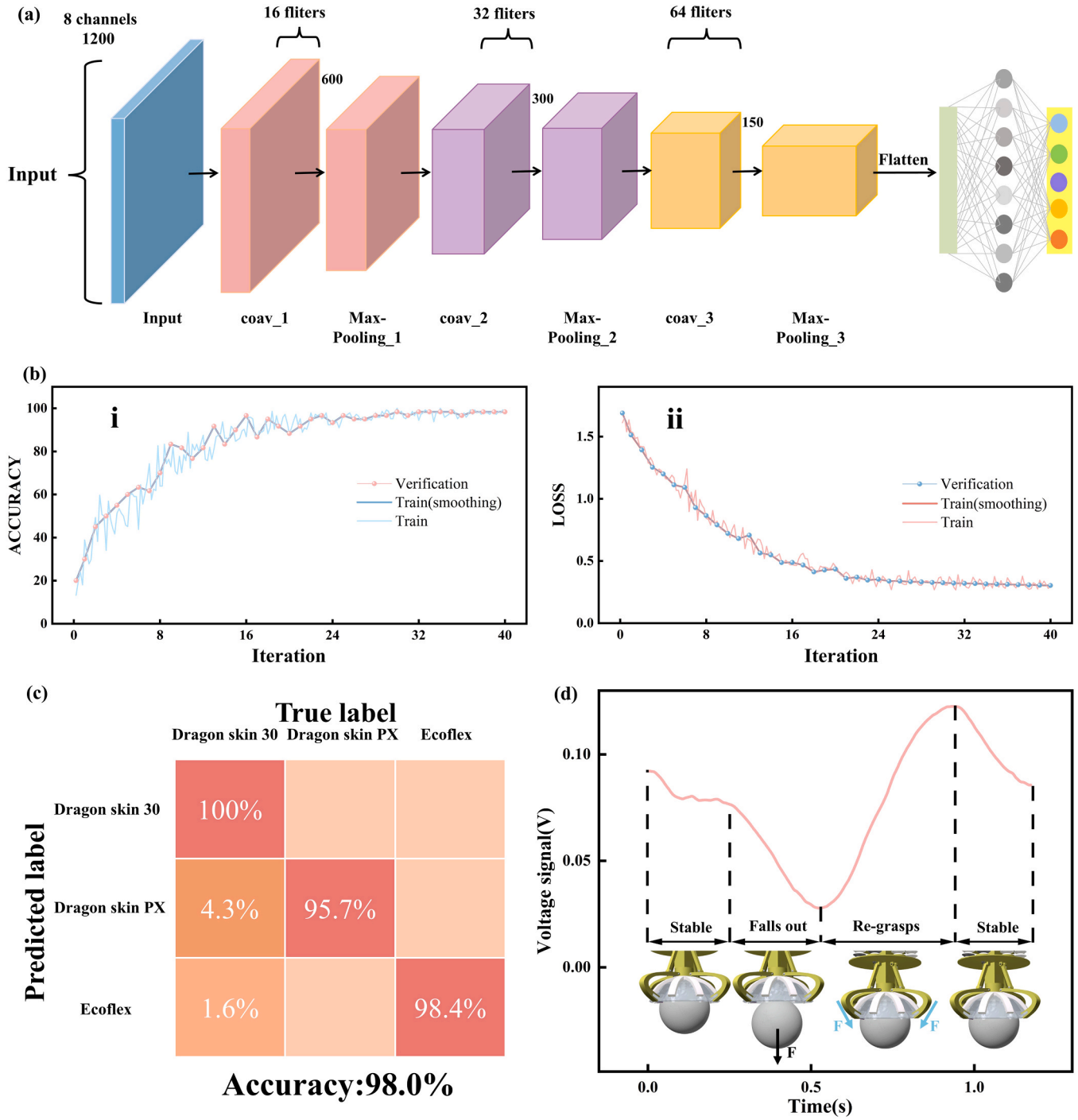

Fig. 5. The model combining CNN and deep learning of UOTG, and the experiment of detecting object detachment. a Basic structure diagram of the CNN training model. b Training progress and loss diagram of deep learning. c Hardness identification confusion matrix. d The experiment of detecting object detachment.

primary vibration frequency band of the sensing unit is concentrated around 0–2 Hz, demonstrating that the sensor's signal is predominantly distributed in the low-frequency range, a pattern consistent with the inherent characteristics of TENG. As the material hardness decreases, the overall energy level experiences a slight reduction (Fig. 4c i-iii), which can be attributed to the fact that harder materials induce greater friction or deformation of the sensing unit during the grasping process, leading to stronger signals. Additionally, slight variations in response intensity across different sensing units are observed, likely due to manufacturing tolerances, positional differences of the object, or environmental factors. However, the overall trend remains consistent, indicating the stable performance of the TENG sensor across various grasping scenarios. These findings further confirm that the TENG sensing unit effectively distinguishes the grasping interactions of materials with different hardness levels, with harder materials producing relatively higher energy signals. The time-frequency characteristics presented here offer a potential method for identifying object hardness, which can aid in optimizing soft grippers for enhanced tactile perception and adaptive grasping strategies.

Relying solely on the voltage value to distinguish the hardness of an object is clearly unreliable. To validate the UOTG's capability in object hardness identification, a deep learning-based model incorporating a convolutional neural network (CNN) architecture was developed [36, 37]. The model inputs eight-channel signals, with each channel containing 1200 sampling points. A total of 100 samples are collected for each of the three hardness levels, with 70 % used for training and 30 % for validation. The training process utilizes MATLAB's deep learning toolbox. Fig. 5a shows the basic structure of the CNN training model used in the experiments. The CNN model comprises an image input layer, three convolutional layers, three pooling layers, one fully connected layer, and one output layer. The output layer selects the softmax function as the activation function. As shown in Fig. 5b, after 40 rounds of training, the model achieved the highest accuracy and demonstrated excellent generalization ability. The confusion matrix in Fig. 5c indicates that the model's recognition accuracy reached 98.0 %.

Additionally, experiments on detecting object detachment and re-grasping were conducted when UOTG grasped the silicone ball. Since the grasping experiment target is a symmetrical object and the sensing units of the device are symmetrically distributed, the output signals of the four sensing units are similar. The sensing unit signal 2 is presented as an example, as shown in Fig. 5d. UOTG is first in a stable gripping state. The signal fluctuates due to the influence of the external environment, but is generally stable. After that, the silicone ball is loosened by external force, resulting in a decrease in the force on the sensing unit, causing its signal to have an obvious falling edge. Then, UOTG re-grips the target when it detects that it is loose. Since UOTG re-grasps the object, the sensing unit is under pressure, resulting in an obvious rising edge. Finally, UOTG remains stable after grasping the object. Since the sensing unit no longer experiences new pressure stimulation after grasping the object, the output signal falls back to the signal range of the stable state.

UOTG can be used to identify the hardness characteristics and shape characteristics of target objects. The shape of the object affects the contact area between the object and the four sensing units, resulting in different voltage signals being generated by each sensing unit during the grasping process. To ensure that the UOTG maintains a constant gripping force when grabbing an object, the pressure of the compressor needs to remain constant. Under this consistent force, the surface pressure is determined by the contact area, causing the UOTG sensing unit to produce distinct signal characteristics when grasping objects of different shapes. By analyzing the signals output by the four sensing units, the shape of the object can be identified. In this experiment, ball, cube, cone, vertical cylinder, and horizontal cylinder (shown as Fig. 6a-c) were selected as the test objects. Under the conditions of a cylinder input pressure of 5 MPa and a grasping frequency of 1 Hz, each object was grasped 12 times consecutively. Fig. 6d illustrates a complete grasping cycle of the UOTG, which includes the preparation for grasping, the grasping process, and the release phase. Fig. 6e-h display the voltage signals from the four sensing units during the grasping of five different objects at the corresponding time intervals. The results show that the same sensing unit produces signals with distinct characteristics when grasping different objects. Notably, for the same object, varying grasping techniques also result in different output signals.

Since the signal manifestations differ when grasping the cylinder vertically and horizontally, separate grasping experiments were conducted for each orientation. In practical applications, by collecting the output signals of the UOTG when grasping different objects, a signal database of object shapes can be established. During grasping tasks, the object's shape can be identified by comparing the signal characteristics of various shapes in the database. The same training model used for hardness recognition is applied for shape recognition. After obtaining the input signal, the corresponding shape of the object can be accurately determined. As shown in Fig. 6i, UOTG achieves an accuracy of 98.3 % in recognizing spheres, cubes, cones, cylinders (vertical), and cylinders (horizontal). This provides a solid foundation for future advancements in underwater intelligent grasping.

Moreover, grasping experiments were conducted on five common underwater creature models, including crabs, sea cucumbers, starfish, pufferfish, and conchs, to evaluate the performance of the UOTG. Under a constant cylinder pressure of 0.3 MPa, the voltage signals generated by sensing unit 1 during the grasping of different creature models are illustrated in Fig. 6j (Detailed photos are in Supplementary Materials Figure S8 - Figure S12). The results demonstrate significant variations in the magnitude and waveform characteristics of the voltage signals across different creature models. These distinct signals indicate that the UOTG exhibits substantial potential for applications in the grasping and identification of diverse underwater creature models.

3. Conclusions

Inspired by the octopus structure, this paper introduces an innovative underwater bionic octopus tactile soft gripper that based on contact-separation triboelectric nanogenerator sensing technology. Through systematic experimental verification and data analysis, the gripper demonstrates the ability to achieve highly sensitive tactile information perception. The gripper can be mounted on ROVs to enhance its ability to detect information about salvaged objects in marine environments characterized by low light conditions and strong interference noise. The key research findings of this paper can be condensed into the following points: 1) Building upon the previous-generation soft gripper [23], the UOTG incorporates structural innovations through multiple improvements, including minimized air leakage in suction cups, a modular and replaceable suction cup design, an optimized gripping mechanism, and significantly enhanced tactile sensing performance. 2) The incorporation of MXene into the ink represents an innovative advancement in TENG materials, significantly enhancing the sensing unit's output performance. 3) UOTG has the ability to distinguish the hardness and shape characteristics of underwater target objects. The recognition accuracy for experimental samples with three different hardness levels is 98.0 %, while the accuracy for experimental samples with five different shapes is 98.3 %. The UOTG exhibits multifunctional performance in both soft grasping and accurate sensing of five common underwater creature models. Distinct waveform signals are generated during interactions with different objects, enabling the establishment of a comprehensive reference database for precise identification. This capability significantly broadens its potential applications in marine environments. 5) The UOTG's recognition capability is fundamentally built on its CNN-driven waveform analysis system, which features an image input layer, three convolutional layers, three pooling layers, one fully connected layer, and one output layer. During a single grasping action, the sensing units generate distinctive waveform electrical signals that encapsulate comprehensive information about the target object.

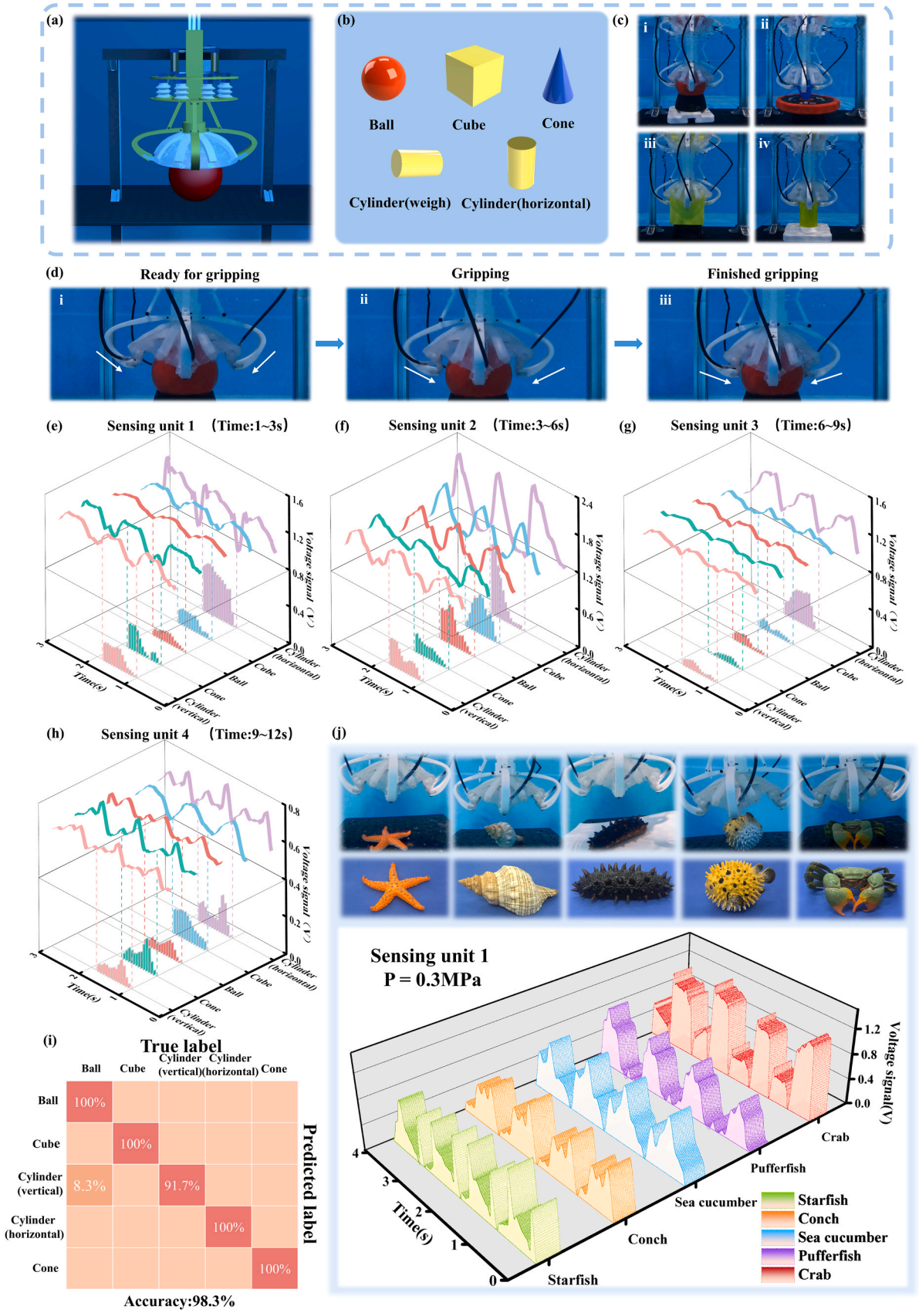

Fig. 6. Underwater shape test device and shape recognition of UOTG. a-c Underwater shape recognition test device of UOTG and the type of recognized objects. d The gipping action process of UOTG. e-h The Output voltage of UOTG when grasping objects of different shapes. i Shape recognition confusion matrix. j Corresponding voltage signals generated by Sensing Unit 1 during the capture of five different underwater creature models at a cylinder pressure of 0.3 MPa.

Through CNN-based pattern recognition, these unique waveforms are analyzed to simultaneously determine the hardness and shape characteristics of the object with high accuracy. When combined with deep learning algorithms, it offers more accurate data support for underwater exploration, enhancing the ability of ROVs to perform underwater grasping and salvage tasks. The research findings demonstrate that UOTG effectively provides underwater robots with perceptual information about grasped targets, highlighting its significant potential in underwater salvage, underwater archaeology, and cleaning up underwater debris.

CRediT authorship contribution statement

Wang Tianrun: Visualization, Validation. **He Weichao:** Writing – review & editing, Software, Methodology, Funding acquisition. **Mou Zhaoyang:** Validation, Software. **Li Jiaqian:** Formal analysis, Data curation. **Xu Peng:** Writing – review & editing, Visualization, Methodology, Funding acquisition, Formal analysis. **Zhou Xinyue:** Methodology, Investigation. **Noor Aziz:** Methodology, Investigation. **XU MINYI:** Writing – review & editing. **Song Liguo:** Writing – review & editing, Methodology. **Li Yuanzheng:** Writing – review & editing, Writing – original draft, Visualization, Validation, Software, Methodology, Formal analysis, Data curation, Conceptualization. **Chen Hongyi:** Writing – original draft, Visualization, Methodology, Investigation, Funding acquisition, Formal analysis, Data curation, Conceptualization.

Declaration of Competing Interest

The authors declare that they have no known competing financial interests or personal relationships that could have appeared to influence the work reported in this paper.

Acknowledgements

This work was supported in part by the National Natural Science Foundation of China [52371345, 52401399, 52071046]; the Xingliao Talent Plan Young Talent Project of Liaoning Province [XLYC2203175]; and the Postdoctoral Fellowship Program of China Postdoctoral Science Foundation [GZC20230062].

Appendix A. Supporting information

Supplementary data associated with this article can be found in the online version at doi:10.1016/j.nanoen.2025.111007.

Data Availability

Data will be made available on request.

References

[1] L. Paull, S. Saeedi, M. Seto, H. Li, Sensor-driven online coverage planning for autonomous underwater vehicles, IEEE/ASME Trans. Mechatron. 18 (2012) 1827–1838.
[2] J. Melo, A.J.O.E. Matos, Survey on advances on terrain based navigation for autonomous underwater vehicles, Ocean Eng. 139 (2017) 250–264, https://doi.org/10.1016/j.oceaneng.2017.04.047.
[3] B. He, H. Zhang, C. Li, S. Zhang, Y. Liang, T.J.S. Yan, Autonomous navigation for autonomous underwater vehicles based on information filters and active sensing, Sensors 11 (2011) 10958–10980, https://doi.org/10.3390/s111110958.
[4] M.V. Jakuba, D. Steinberg, J.C. Kinsey, D.R. Yoerger, R. Camilli, O. Pizarro, S.B. Williams, Toward automatic classification of chemical sensor data from autonomous underwater vehicles, 2011 IEEE/RSJ International Conference on Intelligent Robots and Systems, IEEE, 2011, pp. 4722-4727.
[5] J. Teague, M.J. Allen, T.B. Scott, The potential of low-cost ROV for use in deep-sea mineral, ore prospecting and monitoring, Ocean Eng. 147 (2018) 333–339.
[6] P.I. Macreadie, D.L. McLean, P.G. Thomson, J.C. Partridge, D.O. Jones, A.R. Gates, M.C. Benfield, S.P. Collin, D.J. Booth, L.L. Smith, Eyes in the sea: unlocking the mysteries of the ocean using industrial, remotely operated vehicles (ROVs), Sci. Total Environ. 634 (2018) 1077–1091.
[7] S. Negahdaripour, P.J.I.Jooe Firoozfam, An ROV stereovision system for ship-hull inspection, IEEE J. Ocean. Eng. 31 (2006) 551–564, https://doi.org/10.1109/JOE.2005.851391.
[8] Z. Gong, X. Fang, X. Chen, J. Cheng, Z. Xie, J. Liu, B. Chen, H. Yang, S. Kong, Y. Hao, A soft manipulator for efficient delicate grasping in shallow water: modeling, control, and real-world experiments, Int. J. Robot. Res. 40 (2021) 449–469.
[9] S. Hotta, Y. Mitsui, M. Suka, N. Sakagami, S.J.R.J. Kawamura, Lightweight underwater robot developed for archaeological surveys and excavations, Robomech J. 10 (2023) 2, https://doi.org/10.1186/s40648-023-00240-4.
[10] J.C. Feng, C.R. Li, L. Tang, X.N. Wu, Y. Wang, Z. Yang, W. Yuan, L. Sun, W. Hu, S.J. A.S. Zhang, Tracing the century-long evolution of microplastics deposition in a cold seep, Adv. Sci. 10 (2023) 2206120, https://doi.org/10.1002/advs.202206120.
[11] P. Davies, Y. Reaud, L. Dussud, P.J.O.E. Woerther, Mechanical behaviour of HMPE and aramid fibre ropes for deep sea handling operations, Ocean Eng. 38 (2011) 2208–2214, https://doi.org/10.1016/j.oceaneng.2011.10.010.
[12] A.M. Romanov, N. Gyrichidi, M.P.J.R. Romanov, A novel gripper with integrated rotary unit and force control for pick and place applications, Robotics 11 (2022) 155, https://doi.org/10.3390/robotics11060155.
[13] G. Sun, Z. Wang, Y. Lu, M. Chen, K. Yang, Z. Ni, Underwater laser welding/cladding for high-performance repair of marine metal materials: a review, Chin. J. Mech. Eng. 35 (2022) 5.
[14] M.F. Fallon, J. Folkesson, H. McClelland, J.J. Leonard, Relocating underwater features autonomously using sonar-based SLAM, IEEE J. Ocean. Eng. 38 (2013) 500–513.
[15] G.G. Muscolo, G.J.O.-G. Cannata, A novel tactile sensor for underwater applications: Limits and perspectives, Oceans (2015) 1–7, https://doi.org/10.1109/OCEANS-Genova.2015.7271717.
[16] Z. Zhang, F. Xiang, D. Mei, Y. Wang, Waterproof and flexible aquatic tactile sensor with interlocked ripple structures for broad range force sensing (Adv. Mater. Technol. 2/2024), Adv. Mater. Technol. 9 (2024), https://doi.org/10.1002/admt.202470007.
[17] P. Xu, J. Liu, X. Liu, X. Wang, J. Zheng, S. Wang, T. Chen, H. Wang, C. Wang, X. Fu, G. Xie, J. Tao, M.Jn.F.E. Xu, A bio-inspired and self-powered triboelectric tactile sensor for underwater vehicle perception, NPJ Flex. Electron 6 (2022) 1–10, https://doi.org/10.1038/s41528-022-00160-0.
[18] R.A.S.I. Subad, L.B. Cross, K. Park, Soft robotic hands and tactile sensors for underwater robotics, Appl. Mech. (2021).
[19] J. Zhang, P. Wang, W. Xie, H. Wang, Y. Zhang, H.J.An Zhou, Cephalopod-inspired nanomaterials for optical and thermal regulation: mechanisms, applications and perspectives, ACS Nano (2024), https://doi.org/10.1021/acsnano.4c08338.
[20] H.J. Hoving, B.H. Robison, Vampire squid: detritivores in the oxygen minimum zone, Proc. R. Soc. B: Biol. Sci. 279 (2012) 4559–4567.
[21] S. Johnsen, E.J. Balser, E.C. Fisher, E.A. Widder, Bioluminescence in the deep-sea cirrate octopod Stauroteuthis syrtensis Verrill (Mollusca: Cephalopoda), Biol. Bull. 197 (1) (1999) 26–39.
[22] M. Wu, W.H. Afridi, J. Wu, R.H. Afridi, K. Wang, X. Zheng, C. Wang, G.J.R. Xie, Octopus-inspired underwater soft robotic gripper with crawling and swimming capabilities, Research 7 (2024), https://doi.org/10.34133/research.0456.
[23] M. Wu, X. Zheng, R. Liu, N. Hou, W.H. Afridi, R.H. Afridi, X. Guo, J. Wu, C. Wang, G.J.A.S. Xie, Glowing sucker octopus (Stauroteuthis syrtensis)-inspired soft robotic gripper for underwater self-adaptive grasping and sensing, Adv. Sci. 9 (2022) 2104382, https://doi.org/10.1002/advs.202104382.
[24] M. Lin, M. Vatani, J.-W. Choi, S. Dilibal, E.D.J.S. Engeberg, P. Actuators. A, Compliant underwater manipulator with integrated tactile sensor for nonlinear force feedback control of an SMA actuation system, Sens. Actuators A 315 (2020), https://doi.org/10.1016/j.sna.2020.112221.
[25] Z.L. Wang, J. Chen, L.J.E. Lin, E. Science, progress in triboelectric nanogenerators as a new energy technology and self-powered sensors, Energy Environ. Sci. 8 (2015) 2250–2282, https://doi.org/10.1039/C5EE01532D.
[26] F.-R. Fan, Z.-Q. Tian, Z.L.J.Ne Wang, Flexible triboelectric generator, Nano Energy 1 (2012) 328–334, https://doi.org/10.1016/j.nanoen.2012.01.004.
[27] Z.L. Wang, T. Jiang, L.J.N.E. Xu, Toward the blue energy dream by triboelectric nanogenerator networks, Nano Energy 39 (2017) 9–23, https://doi.org/10.1016/j.nanoen.2017.06.035.
[28] H. Zou, L. Guo, H. Xue, Y. Zhang, X. Shen, X. Liu, P. Wang, X. He, G. Dai, P. Jiang, Quantifying and understanding the triboelectric series of inorganic non-metallic materials, Nat. Commun. 11 (2020) 2093.
[29] S. Wang, P. Xu, J. Liu, H. Wang, J. Si, J. Deng, M. Xu, Z.L. Wang, Underwater triboelectric nanogenerator, Nano Energy 118 (2023) 109018.
[30] X. Wang, Y. Shi, P. Yang, X. Tao, S. Li, R. Lei, Z. Liu, Z.L. Wang, X.J.S. Chen, Fish-wearable data snooping platform for underwater energy harvesting and fish behavior monitoring, Small 18 (2022) 2107232, https://doi.org/10.1002/smll.202107232.
[31] Y. Li, B. Liu, P. Xu, J. Liu, X. Dai, A. Yu, T. Wang, L. Guo, T. Guan, L.J.N.R. Song, A palm-like 3D tactile sensor based on liquid-metal triboelectric nanogenerator for underwater robot gripper, Nano Res. (2024) 1–9, https://doi.org/10.1007/s12274-024-6903-3.
[32] K. Senthil Kumar, Z. Xu, M. Sivaperuman Kalairaj, G. Ponraj, H. Huang, C.-F. Ng, Q.H. Wu, H.J.B. Ren, Stretchable capacitive pressure sensing sleeve deployable onto catheter balloons towards continuous intra-abdominal pressure monitoring, Biosensors 11 (2021) 156, https://doi.org/10.3390/bios11050156.
[33] C.J.Sr Majidi, Soft robotics: a perspective—current trends and prospects for the future, Soft Rob. 1 (2014) 5–11, https://doi.org/10.1089/soro.2013.0001.
[34] D.W. Kim, J.H. Lee, J.K. Kim, U. Jeong, Material aspects of triboelectric energy generation and sensors, NPG Asia Mater. 12 (6) (2020).

[35] B. Mazzolai, A. Mondini, F. Tramacere, G. Riccomi, A. Sadeghi, G. Giordano, E. Del Dottore, M. Scaccia, M. Zampato, S. Carminati, Octopus-Inspired soft arm with suction cups for enhanced grasping tasks in confined environments, Adv. Intell. Syst. 1 (2019) 1900041, https://doi.org/10.1002/aisy.201900041.

[36] L. Zhou, Q. Sun, S. Ding, S. Han, A. Wang, A machine-learning-based method for ship propulsion power prediction in ice, J. Mar. Sci. Eng. 11 (2023) 1381.

[37] L. Zhou, J. Cai, S.J.R.S. Ding, The identification of ice floes and calculation of sea ice concentration based on a deep learning method, Remote Sens. 15 (2023) 2663, https://doi.org/10.3390/rs15102663.